

Failure analysis of fibre metal laminate channel section column under axial compressive pulse loading

Monika ZACZYNSKA *

Department of Strength of Materials, Lodz University of Technology, Stefanowskiego 1/15, 90-537 Lodz, Poland

Abstract. The study aims to analyse the dynamic buckling phenomenon and assess the role of the stress tensor components in the failure process of a short fibre metal laminate column under axial compressive dynamic loading. The investigation is focused on a channel-section profile composed of three aluminium layers and two doubled composite plies [Al/0/90/Al/90/0/Al]. The numerical analysis was performed on the finite element model, which was validated by experimental static buckling tests. Employing a progressive failure algorithm, this analysis incorporated the material property degradation method and Hashin's criterion as the damage initiation criterion. Failure initiation in metal layers was based on the Huber-Mises-Hencky failure criterion. Based on the conducted analyses, it was concluded that the dominant forms of destruction in the FML structure are yielding in the metal layers due to excessive compressive stresses and the failure of the matrix in composite plies as a result of compressive and shear stresses. Through a thorough examination of the stress tensor components, critical stresses contributing to aluminium plastic deformation and laminate failure mechanisms were identified.

Keywords: fibre metal laminates; dynamic buckling; failure analysis; numerical simulations.

1. INTRODUCTION

Nowadays, the engineering approach focuses on applying low-weight materials characterized by high strength. Thus, composite materials and their combination with metal alloys have been used in industries like automotive, wind energy, aviation, etc. [1–3]. The group of materials composed of fibre-reinforced composites and metal alloys is fibre metal laminate (FML) [4]. A metal sheet of aluminium alloy, titanium alloy, or aluminium-lithium alloy can be used, while the composite sheet plays the woven fabrics, aramid-, glass- or carbon-reinforced polymers [5]. One of the most commonly used types of FML in the industry is GLASS REINFORCED LAMINATE (GLARE), which is composed of alternating thin layers of aluminium alloy and glass-fibre-reinforced polymer. The combination of those layers guarantees high impact strength, fatigue strength, damage, and fire resistance. Moreover, GLARE provides a high stiffness-to-weight ratio and strength-to-weight ratio. Alternating layers of different materials makes crack propagation more difficult [6]; thus, high resistance to crack propagation is another benefit of this hybrid structure. GLARE structures have been commercially applied to aircraft parts, such as the upper fuselage skin of the Airbus A380 [7], the front radome bulkhead of the Bombardier Learjet 45 business jet, and the lower flap skins in the Lockheed Martin C-130J Super Hercules military transport aircraft [8].

The aircraft industry demands that designers create as light as possible structures. The introduction of low-weight structures

leads to a weight reduction in construction and decreases operational and manufacturing costs. For this purpose, thin-walled structures are commonly applied. Those structures can withstand significant loads. However, the maximum load of thin-walled aircraft structures is usually restricted not by strength but by stability conditions, thus thin-walled structures are prone to buckling phenomenon. It could occur under static [9–11] and pulse loading [12]. The stability loss problem of thin-walled FML structures subjected to static load has been widely described in the literature.

Bi *et al.* [13] studied the elasto-plastic buckling and post-buckling of the FML plate with initial deflection. Muddappa *et al.* [14] studied the effect of the laminate stacking sequence on the vibration and compression buckling behaviour. Soltani *et al.* [15] investigated the lateral buckling phenomenon in sandwich FML tapered I-beams subjected to transverse loading. The shear buckling phenomenon in FML plates with initial delamination was the aim of a study performed by Niazi *et al.* [16]. Extensive research on the buckling and post-buckling behaviour of an open-section GLARE structure was conducted by Mania *et al.* [17]. The investigation of open cross-section FML columns subjected to static axial compressive force is presented in [17] where the finite element method, experimental tests, and the analytical-numerical method were applied. The aspect of the boundary condition and its effect on the column stability were widely analysed in [20]. A detailed comparison of a classical fibre-reinforced column and a hybrid fibre metal laminate one under compressive loading was presented by Kubiak and Mania in [21]. An attempt to improve the buckling strength of FML columns was performed by Mania and York [22]. The deep failure analysis of GLARE columns subjected to compressive loading was presented by Banat *et al.* [23].

*e-mail: monika.zaczynska@p.lodz.pl

Manuscript submitted 2024-05-07, revised 2024-07-03, initially accepted for publication 2024-07-04, published in September 2024.

Many papers on the dynamic buckling phenomenon in composite thin-walled structures can be found worldwide. As an example, the studies performed by Kubiak [26], Kowal-Michalska [27], Yang [28], and Less and Abramovich [29] can be mentioned. In the literature, only a few papers have been devoted to the hybrid fibre metal laminate structures. Mania [30] investigated GLARE columns under axial compressive impulse loading. The author pointed out the necessity of implementing failure criteria during the dynamic stability assessment of multilayer structures. Zaczynska *et al.* in [32], performed a parametric study on the FML channel section column under pulse loading. To assess the dynamic buckling resistance of the structure, both – deflection dynamic stability criteria and failure criteria were applied.

The stability study of complex thin-walled multilayer structures should include a failure analysis [34]. Numerical simulations seem to be very helpful in identifying the onset of failure initiation and tracking its progression [24]. In fibre metal laminates, metal sheets significantly impact the structure behaviour and response [32]. In the aluminium layer, the unsafe state is related to the material yield. A widely used method to detect the metal yield is tracking the equivalent stress through, i.e. the Huber-von Mises-Hencky criterion [35]. The composite layers with different stacking sequences also affect the damage pattern. The failure could occur in the fibre-reinforced composites (usually prepregs) due to the matrix or fibre cracking. Many continuum-based criteria have been derived to predict the failure in FRP layers. Some are strength-based failure criteria, and some are based on failure mechanisms. A challenging task is to choose the appropriate failure criteria in the investigation of the damage process of FRP plies [23].

Based on the literature overview, there is still insufficient work dedicated to the dynamic stability of FML structures. The prediction of the dynamic response of thin-walled members based on their static buckling assessment is insufficient due to failure processes, which may start locally even for lower dynamic loads. Little work conducted in this regime [30] pointed out the necessity to implement failure criteria to assess the behaviour of FML under pulse loading. Thus, analysing and understanding the various failure mechanisms and their impact on the structure stability under pulse loading seems to be significantly valuable. This work aims to reveal the numerical results of the progressive failure analysis of GLARE channel section columns subjected to axial compressive force. Damages within the thin-walled channel section GLARE columns and their effect on the dynamic buckling stability will be discussed.

2. DYNAMIC BUCKLING

The full transient dynamic analysis in practical FEA enables us to perform a dynamic buckling investigation of the GLARE structure. Kounadis *et al.* [36] found that the damping effect can be neglected in the analysis of dynamic buckling of thin-walled structures under uniform compressive load. Thus, the finite element semi-discrete equation of motion can be expressed as:

$$\{F^a(t)\} = [M] \{\ddot{u}(t)\} + [K] \{u(t)\}, \quad (1)$$

where: $[M]$, $[K]$ – mass and structural stiffness matrix, respectively; $\{\ddot{u}(t)\}$, $\{\dot{u}(t)\}$, $\{u(t)\}$ – nodal acceleration, velocity, and displacement vector, respectively; $\{F^a(t)\}$ – applied load vector.

Nodal accelerations as derivatives of displacements $\{u\}$ regarding time were replaced by displacement differences $\{u\}$ in consecutive discrete moments of time t using the finite difference method. Thus, a new static equilibrium equation was achieved for each time step, taking into account the forces of inertia $[M] \{\ddot{u}\}$. Time integration is performed using the Newmark method and the Newton-Raphson algorithm to solve equations in a consecutive instant of time.

3. FAILURE ANALYSIS

Previous research of the author [32] enhanced the need to include failure criteria dually with deflection dynamic stability criteria, in assessing the resistance of multilayer structures to dynamic pulse loading. Therefore, the analysis of the FML column under pulse loading must include the failure analysis in both components: aluminium sheets and prepreg layers.

3.1. Failure in aluminium layers

In the aluminium layers, the initiation of damage is observed by the plasticity of the material. The well-known Huber-Mises-Hencky (also known as von Mises) criterion is applied to determine the equivalent stresses:

$$\sigma_{eq} = \left(\frac{1}{2} \left[(\sigma_X - \sigma_Y)^2 + (\sigma_Y - \sigma_Z)^2 + (\sigma_Z - \sigma_X)^2 + (\sigma_{XY}^2 + \sigma_{YZ}^2 + \sigma_{ZX}^2) \right] \right)^{1/2}. \quad (2)$$

While reaching equivalent stresses σ_{eq} the magnitude of yield limit $R_{0.2}$, the failure initiates in the aluminium layer, and the material starts to deform plastically. As the material yields, the stiffness reduction occurs, which corresponds to the change of the Young modulus E to the Tangent modulus E_t . For the aluminium layer, the failure factor could be defined as:

$$FF_{Al} = \frac{\sigma_{eqv}}{R_{0.2}}. \quad (3)$$

3.2. Failure in FRP layers

3.2.1. Damage initiation

The Hashin failure criterion is applied as the damage initiation criterion in composite plies. The choice of Hashin's failure criterion was dictated by the growing number of applications in normative issues. Moreover, numerous studies confirm the accuracy of the damage prediction in fibre-reinforced composites [24, 25] with the application of these formulas. Hashin's criterion includes four independent damage modes: fibre tension, fibre compression, matrix tension, and matrix compression, which are described by the following relations (3)–(6):

Fibre tension:

$$FF_F^t = \left(\frac{\sigma_X}{X_t} \right)^2 + \frac{\sigma_{XY}^2 + \sigma_{XZ}^2}{S_{XZ}^2}. \quad (4)$$

Failure analysis of fibre metal laminate channel section column under axial compressive pulse loading

Fibre compression:

$$FF_F^c = -\frac{\bar{\sigma}_1}{X_c}. \quad (5)$$

Matrix tension:

$$FF_M^t = \left(\frac{\sigma_Y + \sigma_Z}{Y_t}\right)^2 + \frac{\sigma_{YZ}^2 - \sigma_Y \sigma_Z}{S_{YZ}^2} + \frac{\sigma_{XY}^2 + \sigma_{XZ}^2}{S_{XY}^2}. \quad (6)$$

Matrix compression:

$$FF_M^c = \frac{1}{Y_c} \left[\left(\frac{Y_c}{2S_{YZ}}\right)^2 - 1 \right] (\sigma_Y + \sigma_Z) + \left(\frac{\sigma_Y + \sigma_Z}{2S_{YZ}}\right)^2 + \frac{\sigma_{YZ}^2 - \sigma_Y \sigma_Z}{2S_{YZ}^2} + \frac{\sigma_{XY}^2 + \sigma_{XZ}^2}{S_{XY}^2}, \quad (7)$$

where: X_t, X_c – longitudinal tensile and compressive strength, Y_t, Y_c – transverse tensile and compressive strength, S_{XY}, S_{YZ} – shear strength in the XY and YZ plane, respectively.

In a damage mechanism, the failure modes can be represented by the degradation of the material stiffness at the lamina level. The heterogeneity of the composite materials means that several damage parameters d must be used [37]. The relationship between the effective stress tensor $\bar{\sigma}_i$ and nominal stress tensor σ_i is given as:

$$\begin{Bmatrix} \bar{\sigma}_1 \\ \bar{\sigma}_2 \\ \bar{\sigma}_6 \end{Bmatrix} = \begin{bmatrix} \frac{1}{1-d_F} & 0 & 0 \\ 0 & \frac{1}{1-d_M} & 0 \\ 0 & 0 & \frac{1}{1-d_S} \end{bmatrix} \begin{Bmatrix} \sigma_1 \\ \sigma_2 \\ \sigma_6 \end{Bmatrix}, \quad (8)$$

where: d_F – fibre damage variable, d_M – matrix damage variable, d_S – shear damage variable.

3.2.2. Material property degradation model (MPDM)

With achieving at least one of the damage factor ($f_f^t, f_f^c, f_m^t, f_m^c$) (see equations (3)–(6)) with the value equal to one indicates the damage in FRP initiates. Then, the gradual reduction of material stiffness for a given damage variable begins. The material property degradation method (MPDM) assumes a gradual decrease in mechanical properties (stiffness) after meeting the initiation damage criterion. Based on the equation (8) and quantitative evaluation of Poisson's degradation coefficient, the damaged elasticity matrix $[D]$ can be expressed as:

$$D = \frac{1}{A} \times \begin{bmatrix} (1-d_F)E_1 & (1-d_F)(1-d_M)\nu_{21}E_1 & 0 \\ (1-d_F)(1-d_M)\nu_{12}E_1 & (1-d_M)E_2 & 0 \\ 0 & 0 & A(1-d_S)G_{12} \end{bmatrix}, \quad (9)$$

where: $A = 1 - \nu_{12}\nu_{21}(1-d_F)(1-d_M)$.

Damage variable coefficient for fibre and matrix damage are independent, and they may have different values depending on

the loading direction (tension or compression), while shear damage variable is the function of the remaining damage variables:

$$d_F = \begin{cases} d_F^t & \text{for } \bar{\sigma}_1 \geq 0, \\ d_F^c & \text{for } \bar{\sigma}_1 < 0, \end{cases} \quad (10)$$

$$d_M = \begin{cases} d_M^t & \text{for } \bar{\sigma}_2 \geq 0, \\ d_M^c & \text{for } \bar{\sigma}_2 < 0, \end{cases} \quad (11)$$

$$d_S = 1 - (1 - d_F^t)(1 - d_F^c)(1 - d_M^t)(1 - d_M^c). \quad (12)$$

The damage variable parameter d equal to zero means no stiffness reduction decrease after damage initiation and $d = 1$ is a complete stiffness loss in the affected mode [38].

In the present work, it was assumed that $d_F^t = d_F^c = d_M^t = d_M^c = 0.9$ and from equation (12) $d_S = 0.9999$. Based on the literature review and the experience of the colleagues in our research group [24] working on the same structures, it was found that the best correlation with the experimental results was obtained for high values of the damage parameter $0.8 < d < 1$.

4. THE OBJECT OF THE STUDY

The subject of the study is a short thin-walled channel section column. The structure is made of FML (GLARE type), composed of three layers of 2024-T3 aluminium alloy and two doubled layers of unidirectional glass-epoxy fibre reinforced prepreg TVR 380 600 M12 26% R-glass. The mechanical and strength properties of the used material were determined experimentally and analytically [40], and presented in Table 1. The total thickness of the structure is equal to $t = 1.94$ mm, where the thickness of individual aluminium sheet $t_{al} = 0.30$ mm and the composite layer $t_p = 0.26$ mm. The overall dimensions of a column are a height of 300 mm, a flange width of 40 mm, a web width of 80 mm, and a corner radius between two adjacent walls of

Table 1

Mechanical and strength properties of FML constituents

TVR 380/26%	Value	Al 2024-T3	Value
E_1 [GPa]	53.90	E [GPa]	77
E_2 [GPa]	14.92	ν [-]	0.3
$\nu_{12} = \nu_{13}$ [-]	0.28	G [GPa]	29.6
ν_{23} [-]	0.40	E_{tang} [MPa]	770
$G_{12} = G_{13}$ [GPa]	5.49	$R_{0.2}$ [MPa]	359
G_{23} [GPa]	5.33		
X_t [MPa]	1534		
X_c [MPa]	800		
Y_t/Z_t [MPa]	75		
Y_c/Z_c [MPa]	500		
S_{XY}/S_{YZ} [MPa]	58		

approximately 1.75 mm (Fig. 1). The selected structure characterized by symmetric layer arrangements [Al/0/90/Al/90/0/Al] was chosen for the analysis. This layer lay-up is a standard grade used in industry and is commercially known as GLARE 3. In the analysis, it is indicated as a C1 channel.

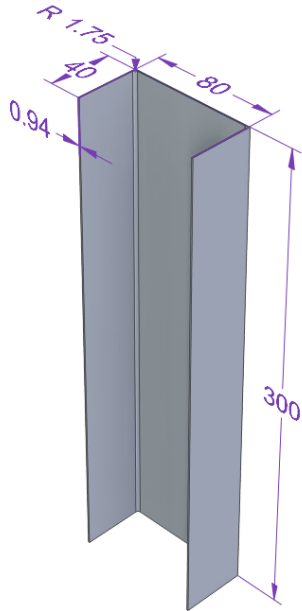


Fig. 1. Dimensions of the column

4.1. Numerical model

Numerical analysis was performed with commercial software ANSYS 2021 R2 [39] based on the finite element method. The column was modelled using SHELL181, i.e. a four-node shell element type with six degrees of freedom at each node. SHELL181 follows the Mindlin-Reissner shell theory and is commonly employed in the modelling of multilayer thin-walled structures. The shell element and section options in the finite element application allow for the independent definition of individual plies of the laminate, including their thickness, material properties, and the main axes of orthotropy. The FE model was divided into a mesh of 3666 elements, determined based on the author's previous experience and the convergence analysis [32]. The convergence of the solution was based on the analysis of the structure deformation. The boundary conditions were applied to reflect those ensured during the experimental static buckling test [19], as presented in Fig. 2a. Thus, displacement perpendicular to the web and flange, as well as the axial displacement of the end of the column bottom edge were blocked. Moreover, a uniform displacement was applied to all nodes located on the upper edges of the column in the axial direction $U_z = \text{const}$. At this end also, the axial compressive load was applied. During the experimental tests (Fig. 2b), the samples were placed in the experimental stand into the special grip with shallow grooves. Therefore, at both edges of the column at a distance equal to the groove depth, the displacement perpendicular to the channel wall was set to zero.

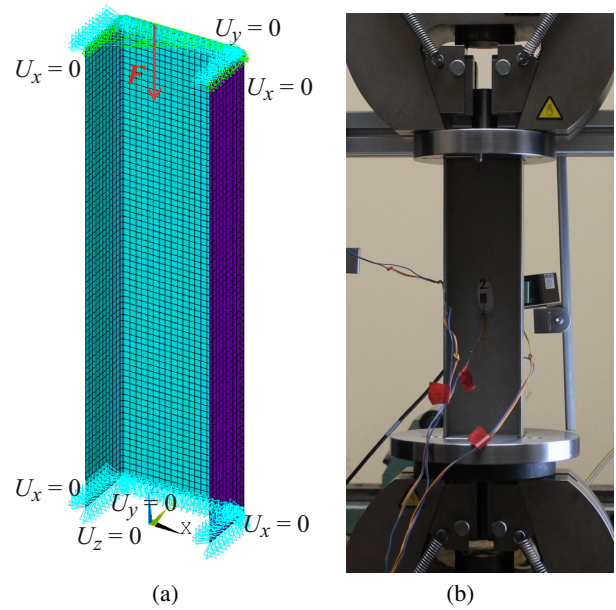


Fig. 2. (a) Numerical model of FML column, (b) specimen in the experimental stand

5. METHODOLOGY OF THE STUDY

The dynamic buckling analysis was performed in ANSYS software and is composed of three stages:

a) Static buckling analysis

Firstly, the linear eigenvalue problem was solved using the Block-Lanczos method. The critical buckling force P_{cr} and corresponding to it the buckling mode shape were determined. Then, the nonlinear static problem was solved with the Newton-Raphson algorithm. Initial geometric imperfections with the shape corresponding to the lowest buckling mode and the amplitude equal to 10% of the total column thickness were applied. The magnitude of the initial imperfection amplitude was set based on the parametric study (details in [32]). The results of FE computations were confronted with laboratory outcomes. The experimental compression tests were carried out using an Instron universal test stand, upgraded with Zwick-Roel control software. The load was introduced by a displacement – a moving of the transverse beam of the machine with constant velocity. The corresponding compressive force was measured with the force sensor. To maintain quasi-static conditions during the test, the machine transverse beam moved at a constant velocity of 1 mm/min. The specimen was positioned in a unique test stand with milled grooves to prevent lateral displacement of the loaded edges, ensuring simply supported boundary conditions. Strain gauges were glued to both sides of the web at the midpoint of its width and height, to monitor the structural response under compressive load. These locations were chosen because they correspond to the predicted amplitudes of section wall buckles during the compression buckling test. Each strain gauge was connected to a single channel of the HBM QuantumX strain bridge using a three-wire system to register its signal. Additionally, a digital image correlation system, Aramis®, was used in the experimental test to track

the deflection of the examined samples. This system allowed for the tracking of the deformation of the entire column, enabling the determination of the buckling mode.

b) *Modal analysis*

The dynamic stability phenomenon is related to stability under time-dependent loads, where the pulse duration is close to the period of natural flexural vibrations [42]. Thus, modal analysis was conducted to determine the period T of fundamental natural flexural vibrations of the FML column.

c) *Dynamic buckling analysis*

The implicit Newmark time integration method was applied to solve the transient analysis for the analysed second-order system. Initial geometrical imperfections corresponding to the buckling mode with the amplitude $w_0 = 0.1t$ were applied. The column was loaded with the rectangular-shaped pulse axially compressive load. The value of pulse amplitude referred to the critical buckling load obtained from LBA (linear buckling analysis) and was in the range $P_0 = (0.4-1.6)P_{cr}$. The pulse load duration was equal to the period of natural vibration T , whereas the column response was traced twice the time of load application (i.e. $t = 2T$). Zero velocity was assumed for the initial conditions. To refer the magnitude of dynamic pulse load to static buckling force, the dynamic load factor (DLF) was introduced as a quotient of applied pulse magnitude (P_0) to static buckling load (P_{cr}). Its critical value was determined by dynamic buckling criteria and/or failure criteria. The application of these two groups of criteria allows one to assess the dynamic stability behaviour of the GLARE column with reference to the material of which it was made, too. Among the well-known dynamic buckling criteria, the Budiansky-Hutchinson and Volmir criteria were chosen, which refer to dynamic buckling to plate/wall deflection. Additionally, the Petry-Fahlbusch dynamic stability criterion (equivalent to the Huber-Mises-Hencky failure criterion) was used for aluminium sheets, and the Hashin failure criterion for FRP layers. In addition to the above-mentioned methods the material property degradation model with reduction of stiffness of FRP layers after the failure initiation was implemented in the analyses as well.

6. RESULTS AND DISCUSSION

6.1. Static buckling and modal analysis

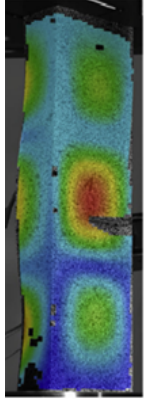
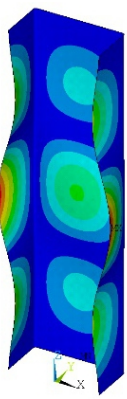
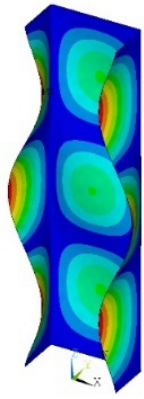
The numerical static buckling test was conducted and compared with the results of a laboratory test. Natural frequencies and their corresponding modal modes were determined through FE modal analysis. The pulse duration, denoted as T , was assumed to be equal to the period of the fundamental natural flexural vibrations of the fifth modal mode ($T = 1/f_5$, where f_5 is the fifth natural frequency of the column). The fifth modal mode corresponds to the lowest buckling mode and periods corresponding to the first four modal modes – thus pulse durations – provide a quasistatic response to dynamic excitation.

In Table 2, a comparison of results is presented for buckling and modal analyses. The buckling load was determined

from laboratory tests using force-deflection data from strain gauge measurements and several methods, including the P-w method, the P-w² method, the Koiter approach, and the inflection point method [43]. The average value of the experimentally determined buckling load was then compared with the buckling load obtained from linear buckling analysis by the numerical method (FEA). The buckling modes were also confronted. The results presented in Table 2 depict a high agreement between the buckling and modal mode data. The experimentally determined critical buckling load is slightly higher compared to the numerical results. The buckling and modal modes obtained by the numerical methods are in agreement with the experimental results.

Table 2

Results of buckling and modal analyses

	Buckling analysis		Modal analysis
	EXP	FEM	FEM
Buckling mode/ modal mode			
Buckling load P_{cr} [N]	31 434	29 384	
Period of natural frequency T [ms]			0.930

6.2. Dynamic buckling analysis

Numerical analyses were conducted for the numerical model with implemented material degradation model, i.e. plastic mechanism in aluminium layers and gradual stiffness reduction in FRP layers. Based on the results of the computations, the change of column deflection with an increase in pulse load amplitude was studied. The maximum deflection of the flange was tracked during the column response because the maximum deflections of the flanges are higher than those of the web. The maximum deflection of the flange observed during the dynamic buckling analysis is indicated as parameter U_{xmax} . However, the localization of the highest deflection changes during the transient analysis. Thus, it was decided to introduce the second parameter, U_{xLBA} , which indicates the deflection at the point at the flange where the maximum flange deflection was observed in the linear buckling analysis (LBA). This point is located in the column half-height at the free edge of the flange. Both deflection parameters U_{xmax} and U_{xLBA} were normalized with

column wall thickness. The change in non-dimensional deflection with the growth of dynamic load factor (*DLF*) is presented in Fig. 3. Dynamic buckling analysis (*DBA*) results are compared with the column non-dimensional deflection for static buckling analysis (*SBA*). In the dynamic buckling analysis, the maximum deflection is observed at the mid-height of the structure in the flange for low load amplitude ($DLF \leq 0.6$). With the increase in pulse loading magnitude, the maximum deflection changes its localization, and the U_{xmax}/t and U_{xLBA}/t curves do not coincide up to a high load amplitude $DLF \geq 1.4$. A steady increase of column deflection is observed under pulse load in the $0.8 \leq DLF \leq 1.4$ regime, while a further increase in load amplitude leads to the rapid growth of the column deflection. A different behaviour is observed when the column is subjected to static compressive load (*SBA* curves). Dimensionless deflections U_{xmax}/t and U_{xLBA}/t coincide in almost all analysed load ranges – up to $DLF = 1.4$. Under the same magnitude of the load, the deformation of the structure under static loading is virtually twice lower than for the pulse one. Thus, the considered structure seems more sensitive to pulse loading than to static loading. A comparison of the buckling modes under different load amplitudes ($DLF = 1$ and $DLF = 1.6$) and load types (static or pulse) presented in Fig. 3 reveals coincidences in the buckling modes. For all analysed cases, three half-waves in the longitudinal direction were observed.

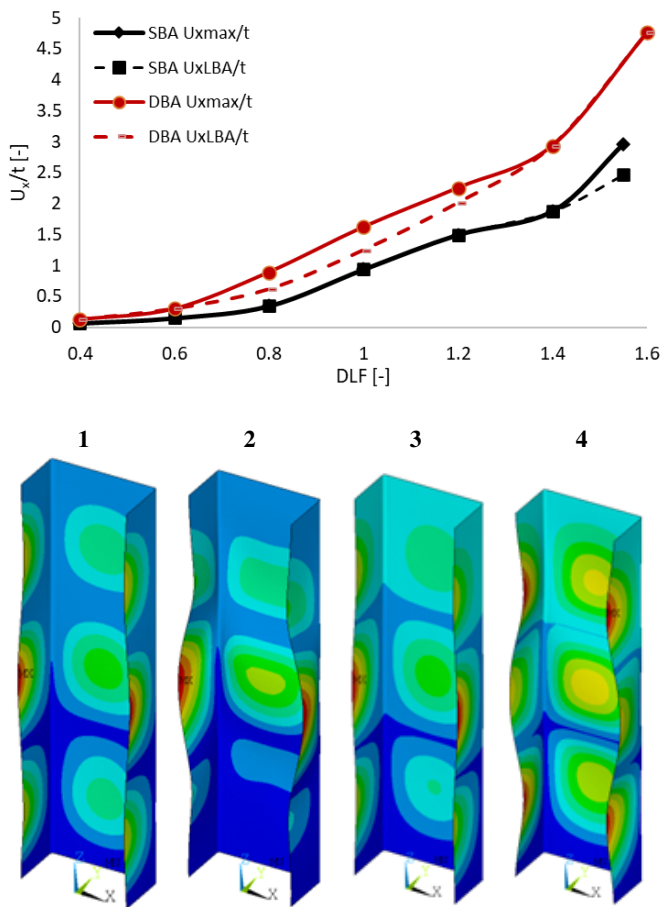


Fig. 3. The change of non-dimensional deflection with the increase of pulse amplitude for the C1 column

Detailed data concerning the column deflection are listed in Table 3. The damaged layers under the considered load amplitude are depicted in red. It should be noted that small, narrow regions near both edges of the column were intentionally omitted from the failure analysis. In those regions, local stress concentration occurs and leads to aluminium yielding and composite plies failure under significantly low loading, which blurs the failure analysis of the entire channel. Similar behaviour was also observed during static buckling laboratory tests [20]. Based on the results obtained for pulse loading, it can be concluded that the failure initiates in the composite inner layers under $DLF = 0.8$. The damage also starts in the outside aluminium layers with an increase in pulse load amplitude. When static compressive loading is applied to the FML channel, the failure also initiates in the internal composite layers. However, the damage is observed under higher load amplitude than in the dynamic buckling analysis. Thus, the analysed FML column is more sensitive to pulse loading than to static loading. As the failure initiates in the structure under a significant low load amplitude ($DLF < 1$), it is desirable to analyse the failure process not only the dynamic buckling deflection response.

Table 3

Non-dimensional deflection and damaged layers of the column

SBA			
<i>DLF</i>	U_{xmax}/t	U_{xLBA}/t	Damaged layers
0.4	0.069	0.069	[Al/0/90/Al/90/0/Al] _T
0.6	0.153	0.153	[Al/0/90/Al/90/0/Al] _T
0.8	0.348	0.348	[Al/0/90/Al/90/0/Al] _T
1.0	0.937	0.937	[Al/0/90/Al/90/0/Al] _T
1.2	1.497	1.497	[Al/0/90/Al/90/0/Al] _T
1.4	1.877	1.877	[Al/0/90/Al/90/0/Al] _T
1.55	2.962	2.465	[Al/0/90/Al/90/0/Al] _T
DBA			
<i>DLF</i>	U_{xmax}/t	U_{xLBA}/t	Damaged layers
0.4	0.126	0.126	[Al/0/90/Al/90/0/Al] _T
0.6	0.300	0.300	[Al/0/90/Al/90/0/Al] _T
0.8	0.891	0.616	[Al/0/90/Al/90/0/Al] _T
1.0	1.621	1.246	[Al/0/90/Al/90/0/Al] _T
1.2	2.254	2.011	[Al/0/90/Al/90/0/Al] _T
1.4	2.935	2.935	[Al/0/90/Al/90/0/Al] _T
1.6	4.759	4.759	[Al/0/90/Al/90/0/Al] _T

It should be noted that the failure analysis in composite materials is highly dependent on the applied failure criteria [23]. In the author's previous study, the LaRC03 failure criterion, based on Hashin's failure model and the failure plane concept for the matrix compression from the Puck criterion, was applied. Failure initiation was observed in metal layers when the FRP plies

were damaged under a slightly higher load [32]. The choice of the Hashin failure criterion in the current study is dictated by the fact that, based on the Hashin criterion, it is possible to describe the failure evolution process based on progressive failure analysis, considering a propagating reduction in mechanical stiffness. The reduction of stiffness after detection of the failure mechanism gives the realistic behaviour of the structure under increasing load.

Table 4
Critical dynamic load factor

DLF_{cr}	Dynamic buckling criterium			
	Volmir	Budiansky-Hutchinson	Petry-Fahlbusch	Hashin
SBA	1.02	1.0 – 1.2	1.2 – 1.4	0.8 – 1.0
DBA	0.83	0.8 – 1.0	0.8 – 1.0	0.6 – 0.8

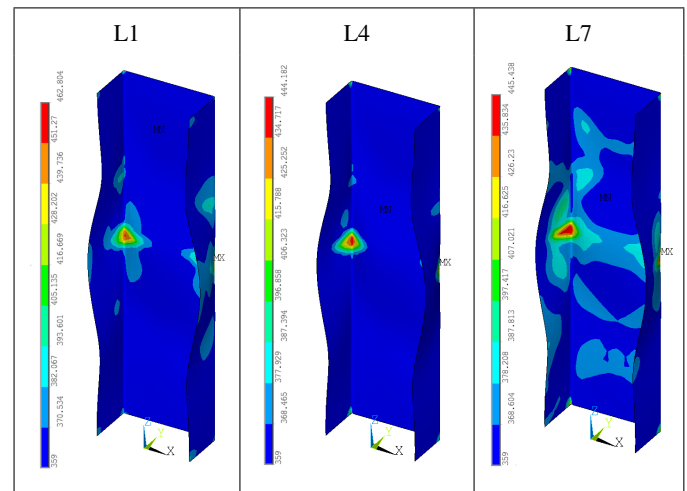
Table 4 displays the critical dynamic load factor values (DLF_{cr}) for the analysed column. This parameter, obtained for a structure under dynamic loading, was compared with results obtained under static loading conditions. Specifically, the Volmir criterion yielded a specified DLF_{cr} value, while the Budiansky-Hutchinson criterion estimated DLF_{cr} as a range of pulse load magnitudes associated with the most rapid deflection increase. In the context of failure criteria, such as the Hashin failure criterion for GFRP plies and the Petry-Fahlbusch criterion for aluminium layers, the load amplitude range leading to failure initiation was chosen as the critical dynamic load factor estimation.

Based on the results presented in Table 4 for dynamic buckling analysis, it can be observed that the dynamic deflection criteria align with the failure criteria for aluminium plies. The Hashin failure criterion, which describes the damage process in composite layers, estimates a slightly lower value of DLF_{cr} . This trend is also noticeable in static buckling analysis; however, under these loading conditions, the Petry-Fahlbusch criterion (being coincident with the Huber-Mises-Hencky criterium) estimates a critical value of the Dynamic Load Factor at a higher level than other criteria. The comparison of results obtained for static buckling analysis (SBA) and dynamic buckling analysis (DBA) also confirms the higher sensitivity of the FML structure to pulse loading. It should be noted that, for both loading conditions, the Hashin failure criteria slightly underestimate the DLF_{cr} parameter. An opposing trend was identified in the author's previous study [32], where the LaRC failure criterion was applied to assess the damage process in composite plies. This underscores the significant influence of the chosen failure criteria on the failure process in FRP plies.

As the failure mechanisms developed in the structure under pulse loading, the failure maps were considered for the selected load amplitude $DLF = 1.6$. Table 5 presents the destruction of the aluminium layers related to the yield stresses. The smallest degraded area occurs in the inner layer L4. After the buckling phenomena occurrence, the middle layer (L4) is subjected to compressive loading, while in the outside layers, additional

bending appears. The highest plastic stresses are observed in the web-flange junction in each considered layer. The connection between the web and the flange is critical in the failure process. Similar conclusions can be found in [25] where the Z-section GLARE columns under static compressive load were analysed. Also in the studies of composite members: I-section structures under tensile loading [44] and top-hat thin-walled columns under compressive loading [45] such a stress distribution was revealed.

Table 5
Failure maps in metal layers under $DLF = 1.6$



The failure maps for the composite layers are shown in Table 6. Similarity in the localization of the damaged area could be observed for L2 and L6 layers and also for L3 and L5 GFRP plies. Damaged areas in the internal GFRP layers are significantly smaller than in the L2 and L6 layers. This behaviour is influenced by high longitudinal stiffness in the inner layers (0°) compared to the outside ones (90°). In the plies with 90° orientation, the highest value of the destruction parameter coincides with the highest yielding stresses in adjacent aluminium layers (L1 and L7 in Table 5). This confirms the dominant role of metal layers in the dynamic response and failure mechanisms of FML structure. In turn, the failure within the GFRP layers aligned longitudinally is developed in the bottom part of the column, near the web-flange junction. High stresses in this part could result from the local stress concentrations in the column edges, as mentioned earlier.

Stress state analysis was performed to investigate the mechanism of failure initiation in the multilayer column subjected to compressive pulse loading. Primarily, the research aims to identify the dominant stress tensor component in the failure process. For this purpose, the numerical calculations were rerun for the model without implementation progressive failure analysis. This allows the stress components to be determined for the nominal (non-degraded) FE model. Directional stresses were selected in the location of damage initiation areas in the column subjected to a load of $DLF = 1$ magnitude. Stress tensor components in aluminium layers (L1 and L7) and composite ones (L3 and L5) listed in Table 7 were used to calculate the components of failure

Table 6

Failure maps in FRP layers under $DLF = 1.6$

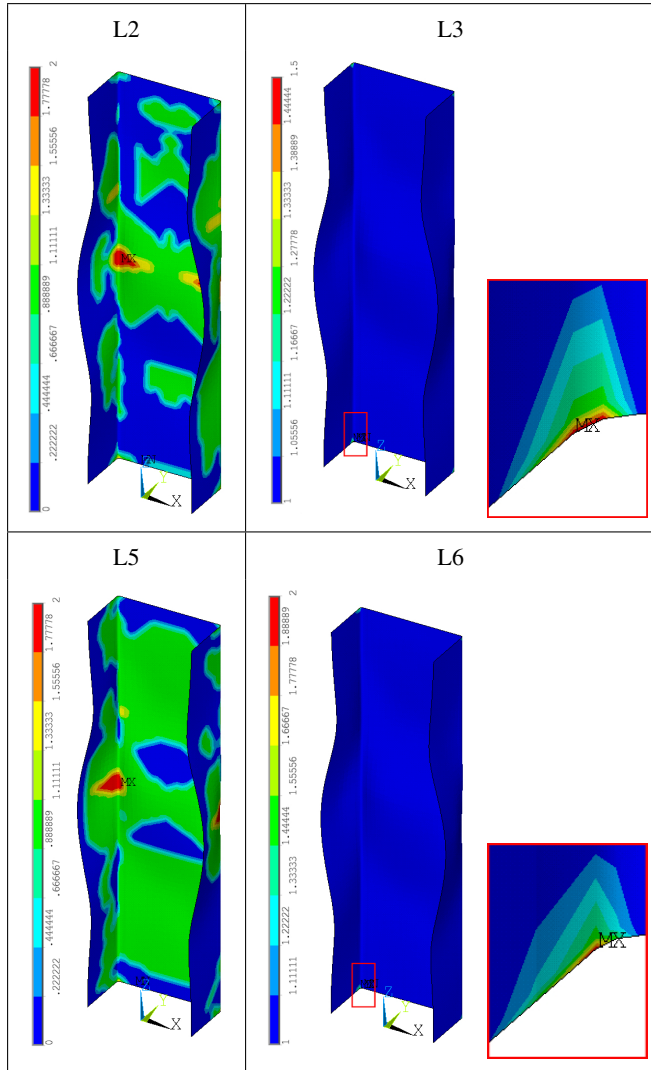


Table 7

Stress tensor components in individual layers under $DLF = 1$

Stress component	Number of the layer			
	L1	L3	L5	L7
σ_X [MPa]	-365.5	-30.8	-31.2	-388.8
σ_Y [MPa]	-13.5	-22.2	-17.2	-68.5
σ_Z [MPa]	-0.3	0.0	0.0	-0.7
σ_{XY} [MPa]	16.2	-1.3	1.5	30.7
σ_{YZ} [MPa]	-1.1	-0.6	0.5	0.3
σ_{XZ} [MPa]	-8.6	-0.2	-0.1	-16.6

Table 8

Aluminium failure factor components

	$\frac{(\sigma_X - \sigma_Y)^2}{2}$	$\frac{(\sigma_Y - \sigma_Z)^2}{2}$	$\frac{(\sigma_Z - \sigma_X)^2}{2}$	$3(\sigma_{XY}^2 + \sigma_{YZ}^2 + \sigma_{ZX}^2)$	FF_{Al}
L1	61941.1	87.0	66671.7	1014.5	1.003
L7	51298.0	2297.2	75305.9	3651.0	1.014

Table 9

Matrix and fibre failure factor components

		L3	L5
Matrix tension failure factor components	$\left(\frac{\sigma_Y + \sigma_Z}{Y_t}\right)^2$	0.088	0.052
	$\frac{\sigma_{YZ}^2 - \sigma_Y \sigma_Z}{S_{YZ}^2}$	0.000	0.000
	$\frac{\sigma_{XY}^2 + \sigma_{XZ}^2}{S_{XY}^2}$	0.002	0.001
	FF_M^t	0.09	0.05
Matrix compression failure factor components	$\frac{1}{Y_c} \left[\left(\frac{Y_c}{2S_{yz}}\right)^2 - 1 \right] (\sigma_Y + \sigma_Z)$	1.085	1.095
	$\left(\frac{\sigma_Y + \sigma_Z}{2S_{yz}}\right)^2$	0.209	0.174
	$\frac{\sigma_{YZ}^2 - \sigma_Y \sigma_Z}{2S_{YZ}^2}$	0.000	0.000
	$\frac{\sigma_{XY}^2 + \sigma_{XZ}^2}{S_{XY}^2}$	0.001	0.001
	FF_M^c	1.29	1.27
Fibre tension failure factor components	$\left(\frac{\sigma_X}{X_t}\right)^2$	0.001	0.002
	$\frac{\sigma_{XY}^2 + \sigma_{XZ}^2}{S_{XZ}^2}$	0.001	0.000
	FF_F^t	0.00	0.00
Fibre compression failure factor components	$-\frac{\bar{\sigma}_1}{X_c}$	0.039	0.039
	FF_F^c	0.04	0.04

factor in the metal layer (equations (2) and (3)) and in the FRP plies (equations (4)–(7)). Results of these analyses are presented in Table 8 for metal plies and in Table 9 for GFRP plies.

Examining the results of the aluminium layer, it can be observed that the stress tensor component σ_X plays a dominant

role in the final failure factor FF_{Al} value, which can be easily explained by the compression type of loading. The remaining stress tensor components have a negligible influence on the failure initiation. However, it can be noticed that in the aluminium outer layer L7, the shear stress tensor component is three times higher than in the L1 layer. Significantly higher values of this component in the L7 layer could be caused by the plasticizing of the layers. The stress tensor components are determined for

the pulse loading leading to the failure so for $FF_{Al} = 1$. With the initiation of the failure process in the aluminium layer, stiffness reduction appears, and the material yields. This leads to an increase in plastic strain magnitude. However, shear stresses are present in the adjacent composite layer (L6) which has higher stiffness than the degraded aluminium layer. This effect is also deepened by the bending effect due to the buckling phenomenon occurrence. For both metal plies, plasticity was observed in the free edge of the flanges near the bottom edge of the structure.

The analogous procedure was performed for the composite layer with the distinction of the matrix FF_M or fibre FF_F failure. Hashin failure criteria distinguish four failure modes: fibre breakage in tension (FF_F^T in equation (4)), fibre buckling in compression (FF_F^C in equation (5)), matrix cracking in tension (FF_M^T in equation (6)) and matrix crushing in compression (FF_M^C in equation (7)). The stress tensor components for both matrix and fibre failure formulas were determined in the same location - the place of the failure initiation of the considered layer. Thus, for both layers L3 and L5, it was the bottom edge of the web near the corners. The stress tensor components (Table 9) show that the matrix component is responsible for the failure of the composite layer. The matrix failure factor FF_M high value corresponds to close to zero fibre failure factor (FF_F) value. The high strength of the fibre results in an almost zero value of the fibre failure factor (Table 1). Matrix crushing generates the failure in the matrix by compression. The dominant stress component in this failure mode is compressive stress σ_Y . High values of compressive stresses σ_Y in combination with the values of transverse compressive strength Y_C and shear strength S_{XY} lead to matrix compression failure. It is in line with observations made by Lapczyk *et al.* [37] and Banat *et al.* [24], who claimed that matrix compressive failure is caused by shear stress. Thus, failure in composite layers is caused by matrix crushing in compression due to a high shear stress state.

7. CONCLUSIONS

The paper presents a failure analysis of a channel section column made of fibre metal laminate subjected to pulse loading. The structure, subjected to axial compressive rectangular-shaped dynamic load, was analysed. Numerical calculations were performed using an experimentally validated finite element model. The numerical calculations were performed with the implementation of the progressive failure algorithm and the application of an implicit Newmark time integration method.

Based on the conducted research, the following conclusions were drawn:

- The column under investigation, under the considered loading conditions, is more sensitive to pulse loading than to static loading. This observation holds true for both deflection and failure analysis, as well as for the determination of the dynamic load factor critical values.
- The area of damage in the outside composite layers corresponds to the yielding area in the adjacent metal sheets, confirming the significant influence of the aluminium layer on the structure behaviour.
- The highest values of the aluminium failure factor FF_{Al} and the composite failure factor FF_M in the outer GFRP plies were observed at the flange-web junction. For inner laminate plies, damage was noted near the bottom edges.
- Stress state analysis in the aluminium layer revealed the highest contribution of compressive stresses to failure.
- Stress state analysis in composite plies determined matrix crushing in compression is the dominant failure mode. This failure mechanism is attributed to the compressive and shear stress components of the stress tensor.

The developed numerical model allows for the analysis of the dynamic buckling phenomenon, taking into account the mechanisms of destruction of the multi-layer FML structure. Thanks to this, it is possible to better understand the impact of laminate destruction forms on the performance of the structure. The research is an attempt to improve the numerical modelling of hybrid layered structures. As a result, it will enable further, fuller use of the potential of these multi-layer structures compared to conventional materials. The numerical model takes into account the progressive destruction of the laminate. The application of analytical formulas in the numerical model facilitated the estimation of the impact of material degradation constants on the dynamic stability of the structure. The implementation of progressive failure analysis facilitated the identification of failure mechanisms in both components of the FML structure.

REFERENCES

- [1] A. Dorigato, "Recycling of thermosetting composites for wind blade application," *Adv. Ind. Eng. Polym. Res.*, no. 5, pp. 116–132, 2021, doi: [10.1016/j.aiepr.2021.02.002](https://doi.org/10.1016/j.aiepr.2021.02.002).
- [2] J. Chroszcielewski, M. Miskiewicz, Ł. Pyrzowski, M. Rucka, B. Sobczyk and K. Wilde, "Modal properties identification of a novel sandwich footbridge – Comparison of measured dynamic response and FEA," *Compos B Eng.*, vol. 151, pp. 245–255, 2018, doi: [10.1016/j.compositesb.2018.06.016](https://doi.org/10.1016/j.compositesb.2018.06.016).
- [3] R. Degenhardt, K. Rohwer, W. Wagner, and J.P. Delsemme, "Postbuckling and collapse analysis of CFRP stringer stiffened panels – a garteur activity," in *Proc. 4th Conf. on Thin-Walled Structures*, Loughborough, England, 2004.
- [4] R.M. Jones, *Mechanics of Composite Materials*, 2nd ed., Philadelphia: Taylor & Francis, 1999.
- [5] J. Sinke, "Development of fibre metal laminates: concurrent multi-scale modelling and testing," *J. Mater. Sci.*, vol. 41, pp. 6777–6788, 2006.
- [6] X. Hao, H. Nie, Z. Ye, Y. Luo, L. Zheng, and W. Liang, "Mechanical properties of a novel fiber metal laminate based on a carbon fiber reinforced Zn-Al alloy composite," *Mater Sci Eng A*, vol. 740–741, pp. 218–225, 2019, doi: [10.1016/j.msea.2018.10.050](https://doi.org/10.1016/j.msea.2018.10.050).
- [7] E. Sherkatghanad, L. Lang, H. Blala, L. Li, and S. Alexandrov, "Fiber metal laminate structure, a good replacement for monolithic and composite materials," *Mater. Sci. Eng.*, vol. 576, pp. 1–9, 2019, doi: [10.1088/1757-899X/576/1/012034](https://doi.org/10.1088/1757-899X/576/1/012034).
- [8] A. Vlot, *Glare: History of the development of a new aircraft material*, Dordrecht: Kluwer Acad. Publ, 2001.
- [9] D. Banat and R.J. Mania, "Stability and strength analysis of thin-walled GLARE composite profiles subjected to axial

- loading,” *Compos. Struct.*, vol. 212, pp. 338–345, 2019, doi: [10.1016/j.compstruct.2019.01.052](https://doi.org/10.1016/j.compstruct.2019.01.052).
- [10] A. Gliszczynski and T. Kubiak, “Load-carrying capacity of thin-walled composite beams subjected to pure bending,” *Thin-Walled Struct.*, vol. 115, pp. 76–85, 2017, doi: [10.1016/j.tws.2017.02.009](https://doi.org/10.1016/j.tws.2017.02.009).
- [11] Z. Zhao, T. Yang, F. Zhang, and P. Ma, “Postbuckling behaviour and failure prediction of large-size composite C-beam under bending-shear coupling load,” *Polymer Compos.*, vol. 44, no. 2, pp. 4266–4278, 2023, doi: [10.1002/pc.27396](https://doi.org/10.1002/pc.27396).
- [12] M. Zaczynska, H. Abramovich, and C. Bisagni, “Parametric studies on the dynamic buckling phenomenon of a composite cylindrical shell under impulsive axial compression,” *J. Sound Vibr.*, vol. 482, p. 115462, 2020, doi: [10.1016/j.jsv.2020.115462](https://doi.org/10.1016/j.jsv.2020.115462).
- [13] R. Bi, Y. Fu, Y. Tian, and C. Jiang, “Buckling and postbuckling analysis of elasto-plastic fiber metal laminates,” *Acta Mech. Solid. Sin.*, vol. 27, no. 1, pp. 73–84, 2014, doi: [10.1016/S0894-9166\(14\)60018-5](https://doi.org/10.1016/S0894-9166(14)60018-5).
- [14] P.P.Y. Muddappa, G. Giridhara, and T. Rajanna, “Buckling behavior of GLARE panels subjected to partial edge loads,” *Mater. Today Proc.*, vol. 45, pp. 94–99, 2021, doi: [10.1016/j.matpr.2020.10.099](https://doi.org/10.1016/j.matpr.2020.10.099).
- [15] M. Soltani and A. Soltani, “An Efficient Approach into Finite Element Method for Lateral Buckling Analysis of Fiber-Metal Laminates Tapered I-Beams,” *Periodica Polytechnica Civil Engineering*, 2022, doi: [10.3311/PPci.18978](https://doi.org/10.3311/PPci.18978).
- [16] M. Niazi and M. Homayoune Sand, “Numerical Shear Buckling Investigation of GLAREs with Initial Delamination,” *Adv. Mat. Sci. Eng.*, vol. 2022, p. 905917, 2022, doi: [10.1155/2022/9059917](https://doi.org/10.1155/2022/9059917).
- [17] R.J. Mania, “Comparative static buckling study of FML thin-walled profiles,” in *ECCM16 – 16th Eur. Conf. Compos. Mater.*, Seville, 2014.
- [18] J. Bienias, R.J. Mania, P. Jakubczak, and K. Majerski, “The issues of manufacturing of geometrically complicated elements by using FML laminates,” *Compos. Theory Pract.*, vol. 15, no. 4, pp. 243–249, 2015.
- [19] R.J. Mania, Z. Kolakowski, and J. Bienias, “Comparative study of FML profiles buckling and postbuckling behaviour under axial loading,” *Compos. Struct.*, vol. 134, pp. 216–225, 2015, doi: [10.1016/j.compstruct.2015.08.093](https://doi.org/10.1016/j.compstruct.2015.08.093).
- [20] D. Banat and R.J. Mania, “Modelling of boundary conditions in Fiber Metal Laminate buckling investigations,” in *Statics, Dyn. Stab. Struct. Buckling Plate Struct. Anal. Numer. Exp. Investig.*, 4th ed., R.J. Mania (Ed.), Lodz University of Technology Series of Monographs, 2016, pp. 49–66.
- [21] T. Kubiak and R.J. Mania, “Hybrid versus FR Laminate Channel Section Columns – Buckling and Postbuckling Behaviour,” *Compos. Struct.*, vol. 154, pp. 142–149, 2016, doi: [10.1016/j.compstruct.2016.07.040](https://doi.org/10.1016/j.compstruct.2016.07.040).
- [22] R.J. Mania and C.B. York, “Buckling strength improvements for Fibre Metal Laminates using thin-ply tailoring,” *Compos. Struct.*, vol. 159, pp. 424–32, 2017, doi: [10.1016/j.compstruct.2016.09.097](https://doi.org/10.1016/j.compstruct.2016.09.097).
- [23] D. Banat and R.J. Mania, “Failure assessment of thin-walled FML profiles during buckling and postbuckling response,” *Compos. Part B-Eng.*, vol. 112, pp. 278–289, 2017, doi: [10.1016/j.compositesb.2017.01.001](https://doi.org/10.1016/j.compositesb.2017.01.001).
- [24] D. Banat, R.J. Mania, and R. Degenhardt, “Stress State Failure Analysis of Thin-Walled GLARE Composite Members Subjected to Axial Loading in the Post-Buckling Range,” *Compos. Struct.*, vol. 289, p. 115468, 2022.
- [25] D. Banat and R.J. Mania, “Progressive Failure Analysis of Thin-Walled Fibre Metal Laminate Columns Subjected to Axial Compression,” *Thin-Walled Struct.*, vol. 122, pp. 52–63, 2022, doi: [10.1016/j.tws.2017.09.034](https://doi.org/10.1016/j.tws.2017.09.034).
- [26] T. Kubiak, “Dynamic buckling of thin-walled composite plates with varying width wise material properties,” *Int. J. Solids Struct.*, vol. 45, pp. 5555–5567, 2005, doi: [10.1016/j.ijsolstr.2005.02.043](https://doi.org/10.1016/j.ijsolstr.2005.02.043).
- [27] K. Kowal-Michalska, “About Some Important Parameters in Dynamic Buckling Analysis of Plated Structures Subjected to Pulse Loading,” *Mech. Mech. Eng.*, vol. 14, no. 2, pp. 269–279, 2010.
- [28] B. Yang, C. Guedes Soares, and D. Wang, “An empirical formulation for predicting the dynamic ultimate strength of rectangular plates under in-plane compressive loading,” *Int. J. Mech. Sci.*, vol. 141, pp. 213–222, 2018, doi: [10.1016/j.ijmecsci.2018.04.015](https://doi.org/10.1016/j.ijmecsci.2018.04.015).
- [29] H. Less and H. Abramovich, “Dynamic buckling of a laminated composite stringer-stiffened cylindrical panel,” *Compos. Part B-Eng.*, vol. 43, pp. 2348–2358, 2012, doi: [10.1016/j.compositesb.2011.11.070](https://doi.org/10.1016/j.compositesb.2011.11.070).
- [30] R.J. Mania, “Dynamic buckling of FML thin-walled panels under axial compression,” in *Stability of Structures XV-th Symposium*, Zakopane, 2018.
- [31] R.J. Mania, “Multi-criterial assessment of dynamic buckling of FML thin-walled profiles,” in *XV Konf. N-T, TKI 2018*, Mikołajki, 2018.
- [32] M. Zaczynska and R.J. Mania, “Investigation of dynamic stability of Fiber Metal Laminate thin-walled columns under axial compression,” *Compos. Struct.*, vol. 271, p. 114155, 2021, doi: [10.1016/j.compstruct.2021.114155](https://doi.org/10.1016/j.compstruct.2021.114155).
- [33] M. Zaczynska and R.J. Mania, “Dynamic stability of thin-walled FML columns including delamination,” *Compos. Struct.*, vol. 290, p. 115478, 2020, doi: [10.1016/j.compstruct.2022.115478](https://doi.org/10.1016/j.compstruct.2022.115478).
- [34] Y. Huang, J. Liu, X. Huang, J. Zhang, and G. Yue, “Delamination and fatigue crack growth behavior in Fiber Metal Laminates (Glare) under single overloads,” *Int. J. Fatigue*, vol. 78, p. 53–60, 2015, doi: [10.1016/j.ijfatigue.2015.04.002](https://doi.org/10.1016/j.ijfatigue.2015.04.002).
- [35] S.P. Timoshenko and J.N. Goodier, *Theory of elasticity*, McGraw Hill Book Company, 1951.
- [36] AN. Kounadis, C. Gantes, and G. Simitses, “Nonlinear dynamic buckling of multi-dof structural dissipative system under impact loading,” *Int. J. Impact Eng.*, vol. 19, no. 1, pp. 63–80, 1997, doi: [10.1016/S0734-743X\(96\)00006-1](https://doi.org/10.1016/S0734-743X(96)00006-1).
- [37] I. Lapczyk and J.A. Hurtado, “Progressive damage modeling in fiber-reinforced materials,” *Compos. Part A Appl. Sci. Manuf.*, vol. 38, pp. 2333–2341, 2007, doi: [10.1016/j.compositesa.2007.01.017](https://doi.org/10.1016/j.compositesa.2007.01.017).
- [38] R. Talreja and C.V. Singh, *Damage and failure of composite materials*, Cambridge, New York: Cambridge University Press; 2012.
- [39] User’s Guide ANSYS®2021 R2, Ansys, Inc., Canonsburg, PA, USA, 2021.
- [40] M. Kamocka, M. Zglinicki, and R.J. Mania, “Multi-method approach for FML mechanical properties prediction,” *Compos. Part B-Eng.*, vol. 91, pp. 135–145, 2016, doi: [10.1016/j.compositesb.2016.01.014](https://doi.org/10.1016/j.compositesb.2016.01.014).

Failure analysis of fibre metal laminate channel section column under axial compressive pulse loading

- [41] M. Kamocka and R.J. Mania, “Assesments methods of mechanical properties of composite materials,” *Mech. Mech. Eng.*, vol. 21, no. 4, pp. 1001–1014, 2017.
- [42] G.J. Simitses, *Dynamic stability of suddenly loaded structures*. New York: Springer–Verlag, 1990.
- [43] M. Paszkiewicz and T. Kubiak, “Selected problems concerning determination of the buckling load of channel section beams and columns,” *Thin-Walled Struct.*, vol. 93, pp. 112–121, 2015, doi: [10.1016/j.tws.2015.03.009](https://doi.org/10.1016/j.tws.2015.03.009).
- [44] A. Quadrino, R. Penna, L. Feo, and N. Nistico, “Mechanical characterization of pultruded elements: Fiber orientation influence vs web-flange junction local problem. Experimental and numerical tests,” *Compos. Part B-Eng.*, vol. 142, pp. 68–84, 2018, doi: [10.1016/j.compositesb.2018.01.001](https://doi.org/10.1016/j.compositesb.2018.01.001).
- [45] P. Rozylo and H. Debski, “Failure Study of Compressed Thin-Walled Composite Columns with Top-Hat Cross-Section,” *Thin-Walled Struct.*, vol. 180, p. 109869, 2022, doi: [10.1016/j.tws.2022.109869](https://doi.org/10.1016/j.tws.2022.109869).